COMMUNICATIONS CHEMISTRY

ARTICLE

DOI: 10.1038/s42004-018-0014-2 OPEN

Hyperthermostable cube-shaped assembly in water

Yi-Yang Zhan[1], Kazuho Ogata[1], Tatsuo Kojima[1], Takuya Koide[2], Kentaro Ishii[3], Takako Mashiko[2], Masanori Tachikawa[2], Susumu Uchiyama[3,4] & Shuichi Hiraoka[1]

Proteins in hyperthermophiles exhibit extremely high thermal stability unlike general proteins. These thermostable proteins are stabilized by weak molecular interactions such as hydrogen bonding, charge interactions and van der Waals (vdW) interactions, along with the hydrophobic effect. An in-depth understanding of the stabilization mechanisms will enable us to rationally design artificial molecules with very high thermal stability. Here we show thermally stable supramolecular assemblies composed of six identical amphiphilic molecules having an indented hydrophobic surface, held together by weak intermolecular interactions (vdW and cation-π interactions) and the hydrophobic effect in water. The disassembly temperature of one of the assemblies is over 150 °C, which is higher than that of the most hyperthermophilic protein reported to date (*Ph*CutA1). Study of the relationship between the structure of the components and the stability of the assemblies indicates that the hyperthermostability is achieved only if all the weak interactions and the hydrophobic effect work cooperatively.

[1] Department of Basic Science, Graduate School of Arts and Sciences, The University of Tokyo, 3-8-1 Komaba, Meguro-ku, Tokyo 153-8902, Japan. [2] Quantum Chemistry Division, Graduate School of Science, Yokohama City University, 22-2 Seto, Kanazawa-ku, Yokohama, Kanagawa 236-0027, Japan. [3] Okazaki Institute for Integrative Bioscience, National Institutes of Natural Sciences, 5-1 Higashiyama, Myodaiji, Okazaki, Aichi 444-8787, Japan. [4] Department of Biotechnology, Graduate School of Engineering, Osaka University, 2-1 Yamadaoka, Suita, Osaka 565-0871, Japan. Correspondence and requests for materials should be addressed to S.H. (email: chiraoka@mail.ecc.u-tokyo.ac.jp)

Unlike the proteins that we generally encounter, which are denaturated by gentle heating, proteins in hyperthermophiles, microorganisms able to survive in temperatures above 80 °C, exhibit extremely high thermal stability. Their stabilization mechanism has attracted much attention[1–9], as these proteins are mainly composed of general amino acids, indicating that the same weak molecular interactions seen in general proteins, such as hydrogen bonding, charge interactions, van der Waals (vdW) interactions and the hydrophobic effect contribute to their high thermal stability. Thus, a deep understanding of these stabilization mechanisms will enable us to rationally design not only new proteins but also novel artificial molecules with very high thermal stability relying only on molecular interactions much weaker than the covalent bond.

Although many efforts have been made in protein engineering using point mutation[10–12] and fragment proteins[13] to reveal this stabilization mechanism in the past two decades, our understanding has not yet reached the point where we can establish a general design principle applicable to a variety of molecular families. Artificial molecular self-assemblies generated with the aid of the hydrophobic effect have also been reported[14–24]. Previously we reported hexameric aggregates of gear-shaped amphiphilic molecules (GSAs) in aqueous methanol[23] and in water[24] under the control of the solvophobic effect and vdW interactions between the components[25].

Here we report a highly thermally stable cube-shaped artificial molecular self-assembly composed of six GSAs in water. Even though the nanocube is assembled solely with the aid of vdW

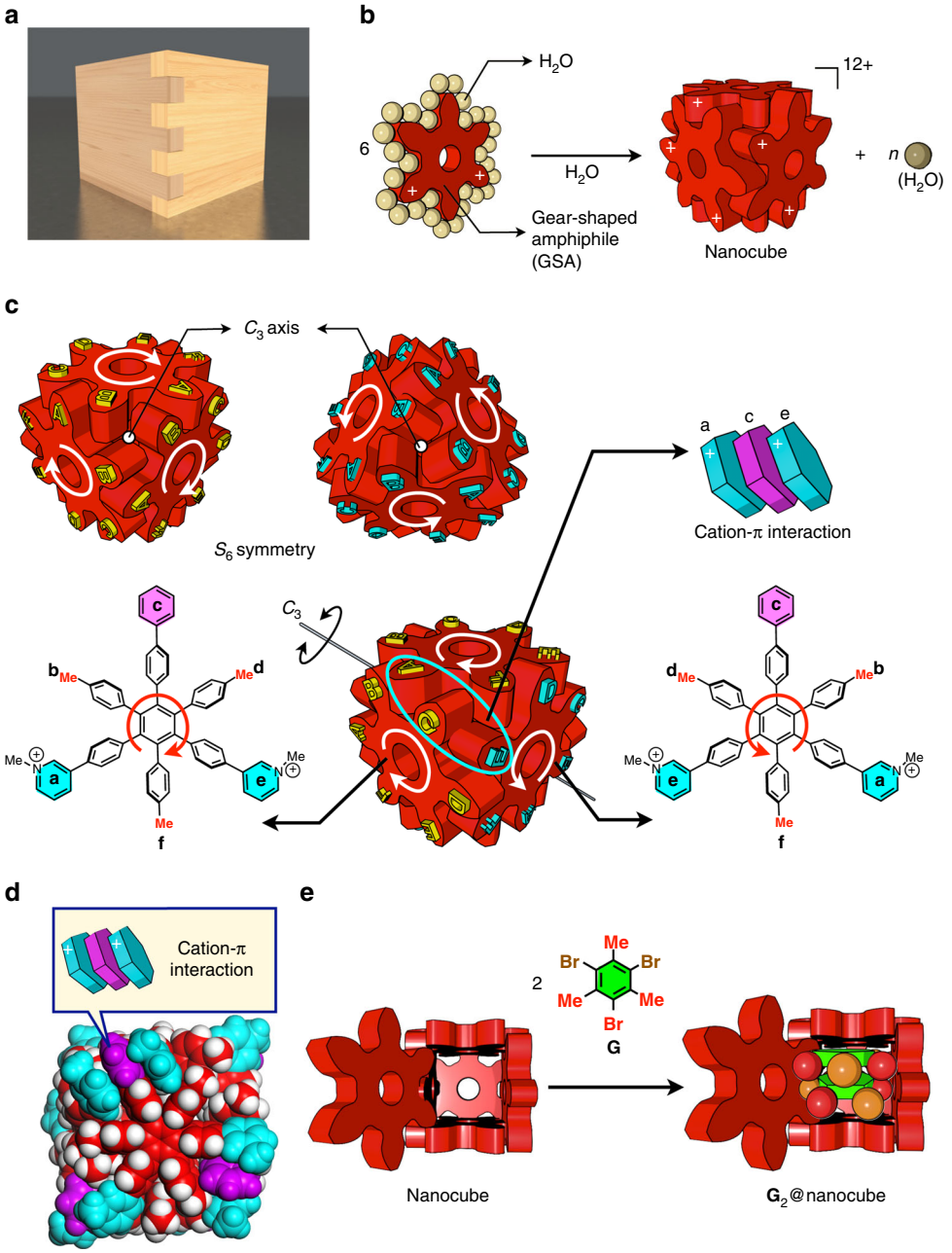

Fig. 1 Design concept and structural features of the nanocube. **a** A photo of a mortise and a tenon, or Hozo, which is traditionally used in Japan for making furniture without the use of nails and glue. **b** A concept of molecular Hozo toward supramolecular structures constructed without directional molecular interactions. The hydrating water molecules on both faces of the GSA are omitted for clarity. **c** The nanocube contains a C_3 axis and has point symmetry, belonging to the S_6 point group. **d** Molecular structure of **BM** nanocube. **e** The nanocube has about a 1-nm-sized inner space, which can be filled with hydrophobic molecules (**G**)

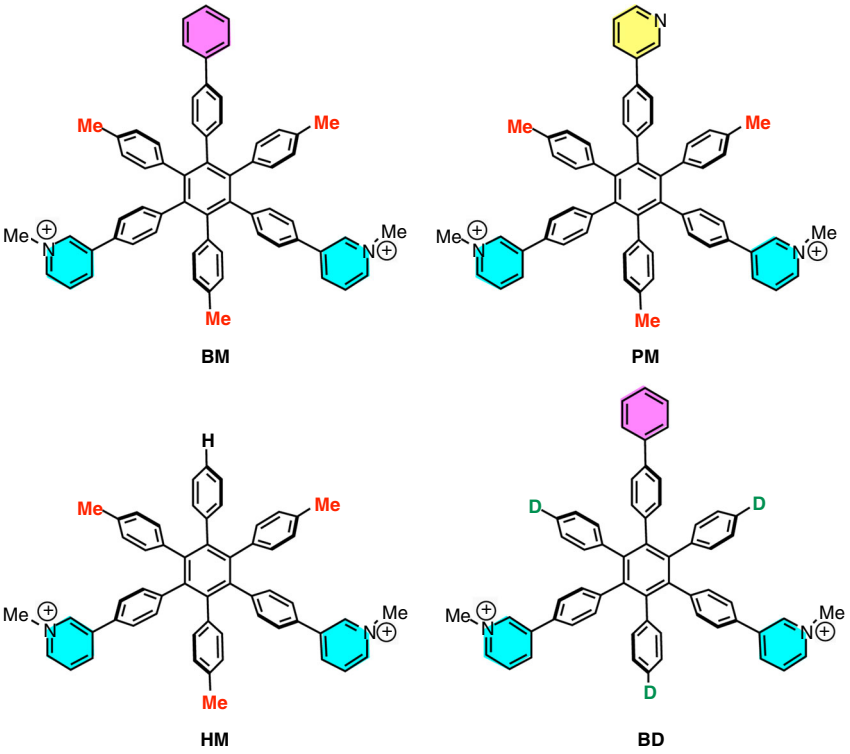

Fig. 2 Chemical structures of gear-shaped amphiphiles. Gear-shaped amphiphiles (GSAs) are hexaarylbenzene derivatives possessing two hydrophilic *N*-methylpyridinium rings (cyan) and hydrophobic substituents on the periphery of a hexaphenylbenzene core. The GSAs have different hydrophobic groups. **BM** contains a benzene ring (magenta) and three methyl groups (red) as hydrophobic substituents. In the same way, **PM** contains a pyridine ring (yellow) and three methyl groups (red), **HM** a hydrogen and three methyl groups (red), and **BD** a benzene ring (magenta) and three deuterium atoms (green)

interactions, cation–π interactions and the hydrophobic effect as in proteins, one of the synthetized nanocube complexes shows higher thermal stability than the most stable thermophilic protein ever reported (*Ph*CutA1)[26], over 150 °C. Comparing the thermodynamic parameters in the GSA library enabled to evaluate the contribution of each molecular interaction to the stability, which emphasized that extremely high thermal stability is realized only when all the molecular interactions and the hydrophobic effect efficiently work together.

Results

Molecular design. Among the stabilizing factors in proteins, the hydrophobic effect much contributes to the stability[27–31]. The hydrophobic effect originates from the desolvation of water molecules upon folding and assembly, and the stabilization free energy linearly decreases with the decrease in the desolvation surface area (ΔSAS)[32]. Van der Waals forces are the weakest molecular interactions involved, but are not negligible when molecular surfaces tightly contact with each other. With such features in mind, in order to attain the hydrophobic contribution effectively and to maximize vdW interactions, we designed a large hydrophobic surface with tight meshing and high complementarity as in a mortise and a tenon, or as in Japanese Hozo, which is a traditional method used to assemble furniture without the use of nails and glue (Fig. 1a, b). Our molecular Hozo, **BM** GSA (Fig. 2), is based on a C_{2v} symmetric hexaphenylbenzene (HPB) framework with three types of substituents on the periphery. Two hydrophilic *N*-methylpyridinium rings (cyan rings in Fig. 2) are introduced so as to endow water-solubility. The shape complementarity between the GSAs in the nanocube can be tuned by alkyl groups (methyl groups and deuterium atoms coloured in red and green, respectively, in Fig. 2). In the nanocube, the benzene ring coloured in magenta in Fig. 2 is placed between the two positively charged *N*-methylpyridinium rings to generate cation–π interactions (Fig. 1c, d), which are often seen in binding sites relating to positively charged species in biological systems[33–35].

Self-assembly of nanocubes in water. **BM** GSA was synthesized from a pentabrominated HPB derivative through the selective alternate lithiation[36, 37] as the key reaction followed by cross-coupling reactions (Supplementary Methods). A ^{1}H NMR spectrum of **BM** GSA in D_2O showed a complicated spectral pattern (Fig. 3b), while that in CD_3OD was perfectly consistent with that of the monomeric **BM** GSA (Fig. 3a), suggesting hydrophobic aggregation of **BM** GSAs in water. ^{1}H DOSY measurement revealed that all the signals show the same diffusion coefficient ($D = 1.51 \times 10^{-10}$ m^2 s^{-1}) (Supplementary Fig. 4), indicating the formation of a single species with a hydrodynamic radius of *ca.* 1.1 nm, which is almost the same as the molecular size of the nanocube. Three chemically inequivalent methyl signals of the tolyl groups coloured in red in Fig. 2 (0.89–1.34 ppm in Fig. 3b) indicate that the GSAs in the aggregate have C_1 symmetry (Fig. 1c), which is consistent with the crystal structure of **PM** nanocube with S_6 point symmetry[24] (Fig. 1c). A large up-field shift of some aromatic and the tolyl methyl protons arising from the shielding effect strongly suggests the molecular meshing between the GSAs in the nanocube composed of six **BM** GSAs.

Thermal stability of nanocubes. The thermal stability of the **BM** nanocube was investigated by variable temperature (VT) ^{1}H NMR measurements. Upon increasing the temperature, only the tolyl signals for the nanocube and for the monomer appeared in an up-field region (Fig. 4 and Supplementary Fig. 22), indicating

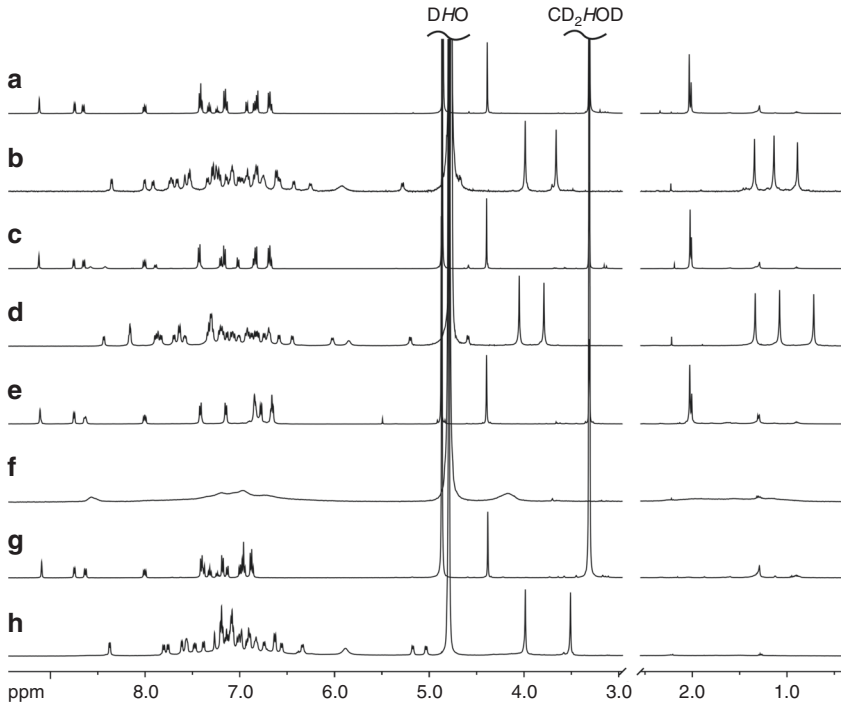

Fig. 3 ^{1}H NMR spectra of GSAs and nanocubes (500 MHz, 298 K, [GSA] = 1 mM). **a BM** GSA in CD_3OD. **b BM** nanocube in D_2O. **c PM** GSA in CD_3OD. **d PM** nanocube in D_2O. **e HM** GSA in CD_3OD. **f HM** nanocube in D_2O. **g BD** GSA in CD_3OD. **h BD** nanocube in D_2O. The assignment of the ^{1}H NMR signals is indicated in Supplementary Figures 1–12

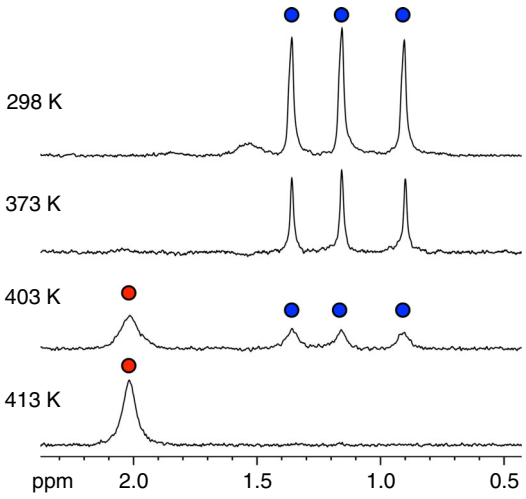

Fig. 4 Partial variable temperature ^{1}H NMR spectra of BM nanocube showing the methyl signals of the tolyl groups (500 MHz, D_2O, [**BM** GSA] = 1.1 mM). Blue and red solid circles indicate **BM** nanocube and **BM** monomer, respectively. The signal of residual DHO at 298 K was used as a reference. The **BM** nanocube and the **BM** monomer were quantified by the integrals of the methyl signals. VT ^{1}H NMR spectra for the other nanocubes are shown in Supplementary Figures 23–29

Table 1 Properties of nanocubes

Nanocube	$T_{1/2}$[a] (K)	$\Delta T_{1/2}$[b] (K)	ΔSAS[c] (Å^2)	ΔC_P[d] (kJ mol^{-1} K^{-1})	PSV[e] (cm^3 g^{-1})
BM	403	-	4258.6	8.01[f]	0.813
G$_2$@BM	>423	>20	5285.3	9.94[f]	0.784
PM	385	-	4220.8	7.94[f]	0.820
G$_2$@PM	408	23	5249.8	9.87[f]	0.787
HM	313	-	3431.0	3.23[g]	0.836
G$_2$@HM	343	30	4383.0	8.24[f]	0.818
BD	338	-	3642.3	6.28[g]	0.831
G$_2$@BD	408	70	4680.1	8.80[f]	0.798

[a]Disassembly temperature ($T_{1/2}$) is the temperature at which half of the nanocubes are disassembled into the monomers, determined by variable temperature ^{1}H NMR spectroscopy. For the nanocubes, $T_{1/2} \neq T_{(\Delta G=0)}$
[b]$\Delta T_{1/2}$ is the difference in the $T_{1/2}$ between the **G$_2$**@nanocube and the nanocube. **G** indicates 1,3,5-tribromomesitylene
[c]Desolvation surface area (ΔSAS) is the difference between the molecular surfaces of the six monomers and that of the nanocube
[d]Heat capacity change for disassembly (ΔC_P) is the difference between C_P of the nanocube state and that of the monomer state
[e]PSV indicates partial-specific volume
[f]Estimated by equation ($\Delta C_P = 1.88 \times$ ΔSAS)[44]
[g]Determined by variable temperature dilution ITC measurements

highly cooperative assembly/disassembly between the two states. In addition, the assembly/disassembly transition was perfectly reversible. The disassembly temperature ($T_{1/2}$) of the **BM** nanocube, at which half of the nanocubes are disassembled into the monomers, is 403 K (Table 1), which is higher than the melting temperature (T_m) of most hyperthermophilic proteins known to us (because different definitions of T_m have been introduced in the previous reports, T_m and $T_{1/2}$ are used separately in this paper). These results clearly indicate that it is possible to construct thermally stable self-assembled structures utilizing only weak molecular interactions and the hydrophobic effect.

Next, in order to evaluate the contribution of each molecular interaction, thermal stability of the nanocubes assembled from GSAs with different substituents introduced on the HPB core (Fig. 2) was investigated (Table 1). When the benzene ring in **BM** GSA (coloured in magenta) is replaced with pyridine (**BM→PM**), whose electrostatic potential surface is slightly less negative than that of benzene, the $T_{1/2}$ of **PM** nanocube (385 K) decreased by 18 K (Supplementary Fig. 24), indicating that the stability of the

nanocubes is very sensitive to the strength of cation–π interactions. Indeed, the nanocube from **HM** GSA, which lacks the benzene ring, showed very broad ^{1}H NMR signals (Fig. 2f), suggesting a less ordered structure, but the formation of the nanocube from **HM** GSA was confirmed by a similar diffusion constant to that of the **BM** nanocube (Supplementary Fig. 8). As expected, the $T_{1/2}$ of **HM** nanocube significantly dropped to 313 K (Supplementary Fig. 26), which is due to the absence of the stabilization from the cation–π interactions, to electrostatic repulsion between the two pyridinium groups and to the decrease in shape complementarity. The replacement of the three methyl groups in the tolyl moieties in **BM** with deuteriums (**BM**→**BD**) also decreased $T_{1/2}$ (338 K) by 65 K (Table 1 and Supplementary Fig. 28), which suggests the importance of shape complementarity.

The thermal stability of the nanocubes was also investigated by differential scanning calorimetry (DSC) measurements (Fig. 5). The transition temperature of **PM** nanocube to the monomers is well consistent with $T_{1/2}$ determined by VT ^{1}H NMR measurements. Because of the temperature limit of the instrument, the transition temperature of **BM** nanocube and a full disassembly profile for **PM** nanocube could not be obtained. As to **HM** and **BD** nanocubes, observation of no apparent peak prevented the determination of the thermodynamic parameters. Although the size of the nanocubes is as small as 2 nm, ΔSAS for the nanocubes ranges from 3400 to 4200 Å^2 (Table 1) and is much larger than that for molecules of a similar size and is comparable to that of small proteins. This is due to the indented hydrophobic surface of GSAs. The stability of the nanocubes well correlates with ΔSAS (Table 1); the larger the ΔSAS, the higher the stability of the nanocube (Supplementary Fig. 50). However, an exception was found between **BM** and **PM** nanocubes. Although the desolvation surface areas for **BM** (4258.6 Å^3) and **PM** (4220.8 Å^3) nanocubes are comparable, $T_{1/2}$ of **BM** nanocube is 18 K higher than that of **PM** nanocube, which suggests that **BM** nanocube is more stabilized by enthalpic contributions from vdW and cation–π interactions.

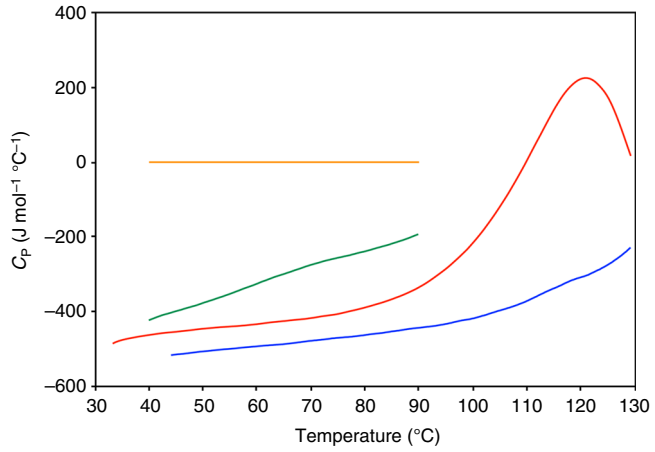

Fig. 5 DSC profiles of nanocubes. Red, blue, green, and orange lines indicate **PM**, **BM**, **BD**, and **HM** nanocubes, respectively

Stability curves of nanocubes. As heat capacity change (ΔC_P) in hydrophobic unfolding and disassembly is positive, the change in the free energy for the disassembly, ΔG_d (T), displays a parabola-shaped curve (stability curve)[38] (Fig. 6a). When ΔC_P is constant,

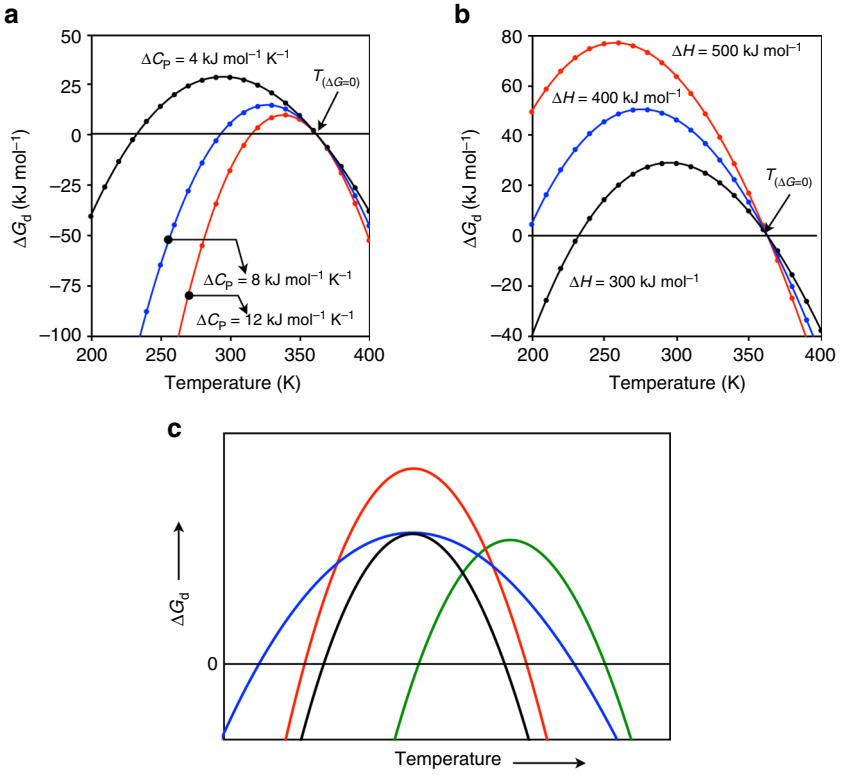

Fig. 6 Case studies of a stability curve for nanocube. The change in the free energy of disassembly with temperature is simulated based on Eq. (1) under the assumption that ΔC_P is constant with temperature. **a** Stability curves with different ΔC_P of disassembly with constant $T_{(\Delta G=0)}$. **b** Stability curves with different $\Delta H(T_{(\Delta G=0)})$ and constant $T_{(\Delta G=0)}$. **c** Three strategies to increase thermal stability. The black line indicates the original stability curve. Lowering the curvature of the black line (blue line) (strategy I), moving the black line up (red line) (strategy II), and moving the black line to the right (green line) (strategy III) increase $T_{(\Delta G=0)}$ to gain higher thermal stability. Although $T_{(\Delta G=0)} \neq T_{1/2}$ for the nanocubes, $T_{1/2}$ also increases with the three strategies

ΔG_d (T) is expressed by Eq. (1):

$$\Delta G_d(T) = \Delta H_d\left(T_{(\Delta G=0)}\right)\left(1 - \frac{T}{T_{(\Delta G=0)}}\right) + \Delta C_P\left(T - T_{(\Delta G=0)} - T\ln\left(\frac{T}{T_{(\Delta G=0)}}\right)\right), \quad (1)$$

where $T_{(\Delta G=0)}$ is the temperature at which $\Delta G_d = 0$. ΔH_d is the enthalpy change for the disassembly of the nanocube. Typical stability curves that are theoretically prepared based on Eq. (1) with constant ΔC_p are shown in Fig. 6. The stability curve suggests that an ordered structure should be destabilized upon decreasing temperature, which is contrary to general intuition. Although Eq. (1) is a theoretical equation that is valid only when ΔC_P is constant with temperature, the destabilisation of proteins at decreasing temperature was truly observed[39, 40]. Figure 6a, b shows the change of the stability curve for a constant $T_{(\Delta G=0)}$ value with varying ΔC_P and ΔH_d at $T_{(\Delta G=0)}$. In hydrophobic unfolding and disassembly, ΔC_P linearly correlates with ΔSAS[41, 42], so the stability curve of the nanocube with large ΔSAS is narrow, indicating a large change in ΔG_d with temperature (Fig. 6a). When ΔH_d at $T_{(\Delta G=0)}$ is large, the stability curve shifts upward with no change of the shape (Fig. 6b). There are three strategies to increase the thermal stability of the nanocube (Fig. 6c): (1) by widening the stability curve (black to blue curves) (strategy I), (2) by shifting the stability curve upward (black to red curves) (strategy II) and (3) by shifting the stability curve toward the right (black to green curves) (strategy III). Thus, the extremely high thermal stability of **BM** nanocube can be discussed by comparing the stability curves of the four nanocubes. To create the stability curve, ΔC_P, $T_{(\Delta G=0)}$ and ΔH_d at $T_{(\Delta G=0)}$ must be determined. It is worth noting that while $T_{(\Delta G=0)} = T_{1/2}$ for the folding of monomeric proteins, in the case of molecular

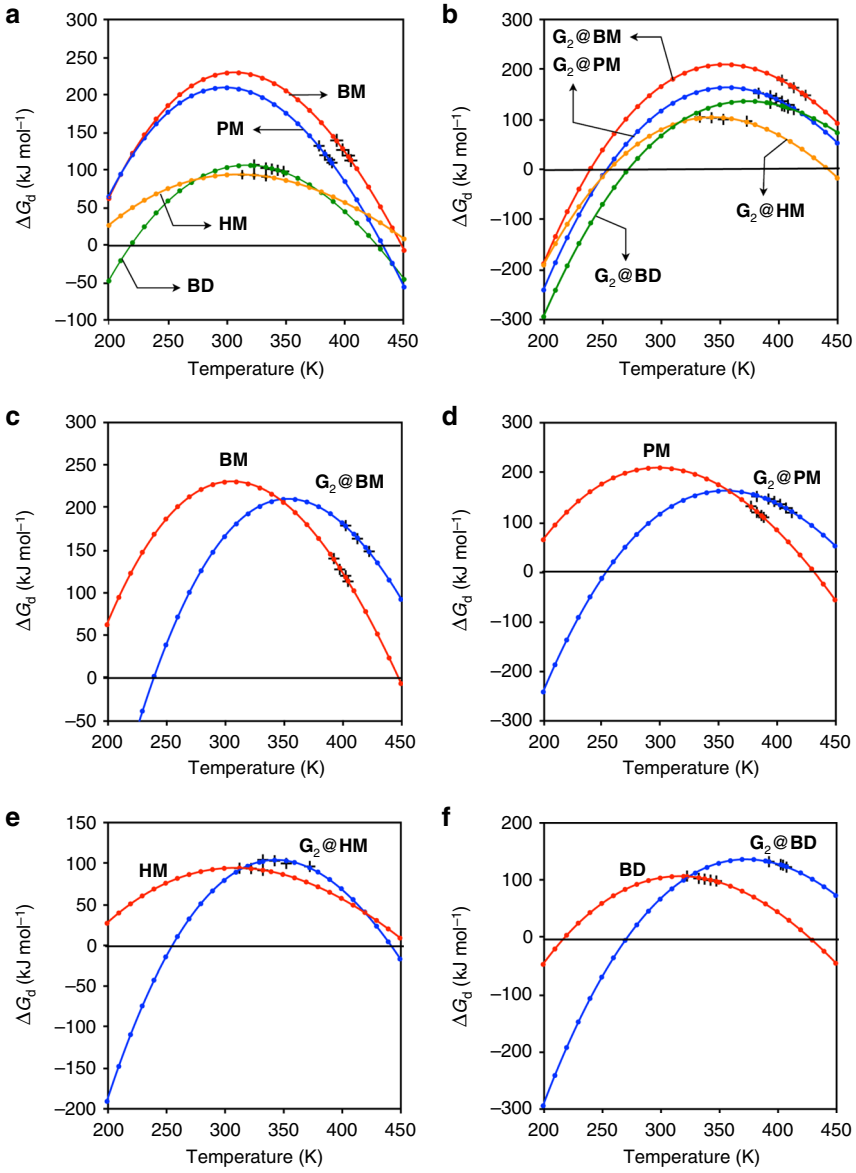

Fig. 7 Plots of ΔG_d of nanocubes with temperature and stability curves. Stability curves were obtained so that Eq. (1) would fit the experimentally obtained ΔG_d values using $T_{(\Delta G=0)}$ and $\Delta H(T_{(\Delta G=0)})$ as variable parameters under the assumption that ΔC_P is constant with temperature. **a** Stability curves of free nanocubes (**BM**, **PM**, **HM**, and **BD**). **b** Stability curves of G_2@nanocubes (G_2@**BM**, G_2@**PM**, G_2@**HM**, and G_2@**BD**). **c**–**f** Effect of encapsulation of guests on the stability of the nanocubes. **c BM** and G_2@**BM**. **d PM** and G_2@**PM**. **e HM** and G_2@**HM**. **f BD** and G_2@**BD**. **G** indicates 1,3,5-tribromomesitylene. Black crosshairs indicate the data obtained by variable temperature ^{1}H NMR spectroscopy

assemblies like nanocubes expressed by Eq. (2), $T_{(\Delta G=0)}$ is not equivalent to $T_{1/2}$.

$$(\mathrm{GSA})_6 \leftrightharpoons 6\,\mathrm{GSA} \quad (2)$$

In addition, in the case of molecular self-assembly, $T_{1/2}$ is a function of the concentration, so $T_{1/2}$ is not an appropriate parameter for the discussion of thermal stability. Thus, $T_{(\Delta G=0)}$, which is not dependent on the concentration, has often been used as T_m of protein assemblies instead of $T_{1/2}$. However, in this paper $T_{1/2}$ at $[\mathrm{GSA\ monomer}]_{total} = 1.0$ mM is defined as the disassembly temperature because most part of the nanocubes are disassembled into the monomers at $T_{(\Delta G=0)}$. It intuitively seems unfair to compare $T_{(\Delta G=0)}$ of the nanocubes with T_m of smaller aggregate of proteins (for molecular self-assemblies, $T_{(\Delta G=0)}$ is higher than $T_{1/2}$).

The ΔC_P values for **HM** and **BD** nanocubes were determined from ΔH values in a certain temperature range (298–308 K), which were experimentally determined by dilution isothermal titration calorimetry (ITC) measurements[43] (Supplementary Tables 3 and 4). On the other hand, the stability of **BM** and **PM** nanocubes is so high that no heat was detected when a concentrated aqueous solution of the nanocubes was added into pure water, which prevented us from determining the ΔC_P values for these nanocubes. The experimentally determined ΔC_P value for **BD** nanocube is well consistent with that estimated by the linear relationship between ΔC_P and ΔSAS ($\Delta C_P = 1.88 \times \Delta$SAS) [44]. However, as mentioned above, because the structure of **HM** nanocube is less ordered, the ΔC_P values determined by the experiment and estimated from the equation contradict each other. For **BM** and **PM** nanocubes, the ΔC_P values were estimated from the equation (Table 1). $T_{(\Delta G=0)}$ and ΔH_d at $T_{(\Delta G=0)}$ were determined so that the stability curve would fit well to the experimentally obtained ΔG_d values. The stability curves of **BM** and **PM** nanocubes are narrower but higher than those for **HM** and **BD** nanocubes (Fig. 7a), indicating that **BM** and **PM** nanocubes were stabilized mainly by enthalpic contributions (strategy II in Fig. 6c). The stability curve of **BM** nanocube lies slightly higher than that of **PM** nanocube, reflecting higher enthalpic stability of **BM**, which would originate from stronger cation–π interactions between the benzene and the pyridinium rings. Considering that the ΔC_P values for **HM** and **BD** nanocubes are smaller than those for **BM** and **PM** nanocubes, the ΔG_d values for **HM** and **BD** nanocubes are less sensitive to temperature, which corresponds to strategy I (Fig. 6c). Indeed, even though the stability curves of **HM** and **BD** nanocubes lie below those of **BM** and **PM** nanocubes, $T_{(\Delta G=0)}$ of **HM** and **BD** nanocubes are similar to those of **PM** and **BM** nanocubes (Fig. 7a).

If we suppose that the GSAs in the nanocube tightly mesh with each other, it is logical to think that they are densely packed. This characteristic can be assessed by partial-specific volume (PSV). A good correlation was found between the stability of the nanocubes and their PSV (Table 1), indicating that a more densely packed nanocube is more stable. Although the structure of **BM** and **PM** GSAs is very similar, the PSV of **BM** nanocube is slightly smaller than that of **PM** nanocube, suggesting that the stronger cation–π interactions in **BM** nanocube slightly tighten the molecular meshing. Compared with proteins, whose PSV[45] ranges from 0.58 to 0.76 $cm^3\,g^{-1}$, the PSV of the nanocubes is relatively high, which indicates that the density of the nanocubes is lower than that of proteins. This is quite reasonable because the nanocubes contain about a 1-nm-sized inner void space. Considering that thermally stable proteins have small void spaces[46], the high thermal stability of **PM** and **BM** nanocubes is surprising, demonstrating that the tight molecular meshing between the GSAs is strong enough to overcome the destabilization coming from having a large void space.

Improvement of thermal stability of nanocubes. The stability of the nanocubes was improved by filling their inner void space with appropriate molecule(s) (Fig. 1e). When 1,3,5-tribromomesitylene (**G**) was added into the nanocube solutions, a couple of **G**s were encapsulated in the nanocubes, which was confirmed by ^{1}H NMR spectroscopy (Supplementary Fig. 16). All the signals for **G** were shifted downfield due to the shielding caused by the aromatic rings of the GSAs. Filling the void space with **G**s decreased the PSV of the nanocubes and $T_{1/2}$ increased of 20–70 K (Table 1). The $T_{1/2}$ of $\mathbf{G}_2$**@BM** is higher than 423 K, at which 20% of the nanocube was disassembled into the monomer (exact $T_{1/2}$ could not be determined because of the temperature limit of our NMR instrument (Supplementary Fig. 23)). $\mathbf{G}_2$**@BM** is thermally more stable than the most stable thermophilic protein ever reported, *Ph*CutA1 ($T_m = 421.5$ K). The less stable **HM** and **BD** nanocubes were additionally stabilized by the encapsulation of the guest molecules (Table 1 and Supplementary Figs. 27 and 29), as a well-ordered nanocube structure was induced from a more fluctuated structure. Upon the encapsulation of the guests, the stability curves for all four nanocubes became similar to each other (Fig. 7b), suggesting that the guest induced the nanocubes to assume a similar shape. All the stability curves of the $\mathbf{G}_2$@nanocubes shifted to the right (Fig. 7c–f), suggesting that filling the void space corresponds to the third strategy to improve the thermal stability (Fig. 6c). The top part of the parabola of **BM** and **PM** nanocubes slightly decreased (Fig. 7c, d), suggesting the decrease in the enthalpic contribution. This is mainly because the volume of two **G**s is slightly larger than the inner space of the nanocube, which causes the molecular meshing between the GSAs to decrease. The nanocubes are thus slightly destabilized enthalpically in the meshing, but additional vdW interactions between the nanocube and **G** enthalpically contributes to the stability. On the other hand, the stability curves for **BD** and **HM** nanocubes rose upon the encapsulation (Fig. 7e, f), which is due to the increase in the molecular meshing between the GSAs caused by the induced-fit to the guests.

Discussion

In conclusion, a self-assembled structure with extremely high thermal stability, **BM** nanocube, was created from gear-shaped amphiphilic molecules based on Hozo with an indented hydrophobic molecular surface utilizing only weak molecular interactions and the hydrophobic effect. As all the nanocubes have large desolvation surface areas (ΔSAS) comparable to those of small proteins, the hydrophobic effect is a driving force of the formation of the nanocube and also much contributes to the stability of this. However, the low stability of **HM** and **BD** nanocubes with large ΔSAS (3431 and 3642 $Å^2$) indicates that other molecular interactions such as vdW and cation–π interactions also play a significant role for the thermal stability. Some thermophilic proteins contain many charged residues (Asp, Glu, Lys, and Arg)[26, 47, 48], suggesting the importance of electrostatic interaction. Likewise, **BM** nanocube, which has slightly stronger cation–π interactions (between the benzene and the *N*-methylpyridinium rings) than **PM** nanocube (which has a pyridine instead of a benzene), has greater thermal stability, which indicates that even slight differences in the electrostatic potential surfaces between benzene and pyridine clearly affect the stability. Molecular meshing, which mainly contributes to vdW interactions between GSAs, is another important factor to increase the thermal stability. Therefore, the extremely high thermal stability of the nanocube is attained only if all the

contributions work together. In other words, for the creation of a highly stable self-assembly or folded structure in water, (1) a desolvation surface area (ΔSAS) of over several thousands Å^3 (the hydrophobic effect), (2) complementary hydrophobic surfaces (vdW interactions), and (3) electrostatic interactions such as cation–π interactions should properly be included in designed molecules. Such new design principles would enable to pave the way toward discrete molecular self-assemblies with high stability in water that can be utilized for the purpose of the interplay with biological molecules under physiological conditions and for industrial purposes such as the transformations of molecules under harsh conditions.

Methods

Synthesis of GSAs. Synthesis of GSAs is detailed in the Supplementary Methods. NMR characterization of GSAs is provided in Supplementary Figures 1–12. ^{1}H and ^{13}C NMR spectra of all the new compounds are provided in Supplementary Figures 51–86.

Mass spectrometry. ESI-MS spectra of nanocubes are provided in Supplementary Figures 13–15 and the observed species are summarized in Supplementary Table 1.

Preparation of nanocube with guests. Preparation of nanocube with guests is detailed in the Supplementary Methods. ^{1}H and ^{1}H DOSY NMR spectra are provided in Supplementary Figures 16–19.

H/D exchange. H/D exchange of nanocubes in D_2O at high temperature is described in the Supplementary Methods. ^{1}H NMR spectra are provided in Supplementary Figures 20 and 21.

Determination of $T_{1/2}$ of nanocubes. Determination of $T_{1/2}$ of nanocubes is detailed in the Supplementary Methods. ^{1}H NMR spectra are provided in Supplementary Figures 22–29 and the data are provided in Supplementary Table 2.

Dilution ITC experiments. Dilution ITC experiments are detailed in the Supplementary Methods. Titration curves are provided in Supplementary Figures 30–40 and the data are provided in Supplementary Tables 3 and 4.

DSC measurement. DSC measurement is detailed in the Supplementary Methods.

Partial-specific volume. Determination of partial-specific volume is detailed in the Supplementary Methods. The results are provided in Supplementary Figures 41–48 and Supplementary Tables 5 and 6.

Desolvation surface area of nanocubes. Computational methods to determine ΔSAS of nanocubes are detailed in the Supplementary Methods. Geometrically optimized structures of nanocubes are provided in Supplementary Figure 49. Plots of the $T_{1/2}$ with respect to the ΔSAS of nanocubes are shown in Supplementary Figure 50. The detailed data of ΔSAS are provided in Supplementary Table 7.

Determination of stability curves for nanocubes. Determination of stability curves for nanocubes is detailed in the Supplementary Methods. The data for the analysis of the nanocubes and the stability curves with the experimentally obtained $\Delta G_d(T)$ are shown in Supplementary Tables 8–15.

Data availability. The authors declare that all the other data supporting the findings of this study are available within the article and its supplementary information files and from the corresponding author upon request.

Received: 7 November 2017 Accepted: 26 January 2018
Published online: 22 March 2018

References

1. Vieille, C. & Zeikus, G. J. Hyperthermophilic enzymes: sources, uses, and molecular mechanisms for thermostability. *Microbiol. Mol. Biol. Rev.* **65**, 1–43 (2001).
2. Jaenicke, R. & Böhm, G. The stability of proteins in extreme environments. *Curr. Opin. Struct. Biol.* **8**, 738–748 (1998).
3. Vetriani, C. et al. Protein thermostability above 100 °C: a key role for ionic interactions. *Proc. Natl Acad. Sci. USA* **95**, 12300–12305 (1998).
4. Korndörfer, I., Steipe, B., Huber, R., Tomschy, A. & Jaenicke, R. The crystal structure of holo-glyceraldehyde-3-phosphate dehydrogenase from the hyperthermophilic bacterium thermotoga maritima at 2.5 Å resolution. *J. Mol. Biol.* **246**, 511–521 (1995).
5. Malakauskas, S. M. & Mayo, S. L. Design, structure and stability of a hyperthermophilic protein variant. *Nat. Struct. Biol.* **5**, 470–475 (1998).
6. Yutani, K., Ogasahara, K., Sugino, Y. & Matsushiro, A. Effect of a single amino acid substitution on stability of conformation of a protein. *Nature* **267**, 274–275 (1977).
7. Pace, C. N., Scholtz, J. M. & Grimsley, G. R. Forces stabilizing proteins. *FEBS Lett.* **588**, 2177–2184 (2014).
8. Karshikoff, A., Nilsson, L. & Ladenstein, R. Rigidity versus flexibility: the dilemma of understanding protein thermal stability. *FEBS J.* **282**, 3899–3917 (2015).
9. Hernandez, G., Jenney, F. E., Adams, M. W. & LeMaster, D. M. Millisecond time scale conformational flexibility in a hyperthermophile protein at ambient temperature. *Proc. Natl Acad. Sci. USA* **97**, 3166–3170 (2000).
10. Tokuriki, N. & Tawfik, D. S. Stability effects of mutations and protein evolvability. *Curr. Opin. Struct. Biol.* **19**, 596–604 (2009).
11. Parthiban, V., Gromiha, M. M. & Schomburg, D. CUPSAT: prediction of protein stability upon point mutations. *Nucleic Acids Res.* **34**, 239–242 (2006).
12. Steinbrecher, T. et al. Predicting the effect of amino acid single-point mutations on protein stability—large-scale validation of MD-based relative free energy calculations. *J. Mol. Biol.* **429**, 948–963 (2017).
13. Rocklin, G. J. et al. Global analysis of protein folding using massively parallel design, synthesis, and testing. *Science* **357**, 168–175 (2017).
14. Gibb, C. L. D. & Gibb, B. C. Well-defined, organic nanoenvironments in water: the hydrophobic effect drives a capsular assembly. *J. Am. Chem. Soc.* **126**, 11408–11409 (2004).
15. Gan, H. & Gibb, B. C. Guest-controlled self-sorting in assemblies driven by the hydrophobic effect. *Chem. Commun.* **48**, 1656–1658 (2012).
16. Gan, H. & Gibb, B. C. Guest-mediated switching of the assembly state of a water-soluble deep-cavity cavitand. *Chem. Commun.* **49**, 1395–1397 (2013).
17. Jordan, J. H. & Gibb, B. C. Molecular containers assembled through the hydrophobic effect. *Chem. Soc. Rev.* **44**, 547–585 (2015).
18. Suzuki, A., Kondo, K., Akita, M. & Yoshizawa, M. Atroposelective self-assembly of a molecular capsule from amphiphilic anthracene trimers. *Angew. Chem. Int. Ed.* **52**, 8120–8123 (2013).
19. Kondo, K., Suzuki, A., Akita, M. & Yoshizawa, M. Micelle-like molecular capsules with anthracene shells as photoactive hosts. *Angew. Chem. Int. Ed.* **52**, 2308–2312 (2013).
20. Kondo, K., Klosterman, J. K. & Yoshizawa, M. Aromatic micelles as a new class of aqueous molecular flasks. *Chem. Eur. J.* **23**, 16710–16721 (2017).
21. Suzuki, A., Akita, M. & Yoshizawa, M. Amphiphilic tribranched scaffolds with polyaromatic panels that wrap perylene stacks displaying unusual emissions. *Chem. Commun.* **52**, 10024–10027 (2016).
22. Cremer, P. S., Flood, A. H., Gibb, B. C. & Mobley, D. L. Collaborative routes to clarifying the murky waters of aqueous supramolecular chemistry. *Nat. Chem.* **10**, 8–16 (2018).
23. Hiraoka, S., Harano, K., Shiro, M. & Shionoya, M. A self-assembled organic capsule formed from the union of six hexagram-shaped amphiphile molecules. *J. Am. Chem. Soc.* **130**, 14368–14369 (2008).
24. Hiraoka, S., Nakamura, T., Shiro, M. & Shionoya, M. In-water truly monodisperse aggregation of gear-shaped amphiphiles based on hydrophobic surface engineering. *J. Am. Chem. Soc.* **132**, 13223–13225 (2010).
25. Koseki, J., Kita, Y., Hiraoka, S., Nagashima, U. & Tachikawa, M. Role of CH-π interaction energy in self-assembled gear-shaped amphiphile molecules: correlated ab initio molecular orbital and density functional theory study. *Theor. Chem. Acc.* **130**, 1055–1059 (2011).
26. Tanaka, T. et al. Hyper-thermostability of CutA1 protein, with a denaturation temperature of nearly 150 °C. *FEBS Lett.* **580**, 4224–4230 (2006).
27. Camilloni, C. et al. Towards a structural biology of the hydrophobic effect in protein folding. *Sci. Rep.* **6**, 28285 (2016).
28. Chandler, D. Interfaces and the driving force of hydrophobic assembly. *Nature* **437**, 640–647 (2005).
29. Levy, Y. & Onuchic, J. N. Water mediation in protein folding and molecular recognition. *Annu. Rev. Biophys. Biomol. Struct.* **35**, 389–415 (2006).
30. Berne, B. J., Weeks, J. D. & Zhou, R. Dewetting and hydrophobic interaction in physical and biological systems. *Annu. Rev. Phys. Chem.* **60**, 85–103 (2009).
31. Huang, D. M. & Chandler, D. Temperature and length scale dependence of hydrophobic effects and their possible implications for protein folding. *Proc. Natl Acad. Sci. USA* **97**, 8324–8327 (2000).

32. Houk, K. N., Leach, A. G., Kim, S. P. & Zhang, X. Binding affinities of host-guest, protein-ligand, and protein-transition-state complexes. *Angew. Chem. Int. Ed.* **42**, 4872–4897 (2003).
33. Dougherty, D. A. Cation-π interaction in chemistry and biology: a new view of benzene, Phe, Tyr, and Trp. *Science* **271**, 163–168 (1996).
34. Baker, E. G. et al. Engineering protein stability with atomic precision in a monomeric miniprotein. *Nat. Chem. Biol.* **13**, 764–770 (2017).
35. Brandl, M., Weiss, M. S., Jabs, A., Sühnel, J. & Hilgenfeld, R. C-H···π-interactions in proteins. *J. Mol. Biol.* **307**, 357–377 (2001).
36. Kojima, T. & Hiraoka, S. Selective alternate derivatization of the hexaphenylbenzene framework through a thermodynamically controlled halogen dance. *Org. Lett.* **16**, 1024–1027 (2014).
37. Kojima, T. & Hiraoka, S. Mesityllithium and *p*-(dimethylamino)phenyllithium for the selective alternate trilithiation of the hexaphenylbenzene framework. *Chem. Commun.* **50**, 10420–10423 (2014).
38. Becktel, W. J. & Schellman, J. A. Protein stability curves. *Biopolymers* **26**, 1859–1877 (1987).
39. Rosa, M., Roberts, C. J. & Rodrigues, M. A. Connecting high-temperature and low-temperature protein stability and aggregation. *PLoS ONE* **12**, e0176748 (2017).
40. Olsson, C., Jansson, H. & Swenson, J. The role of trehalose for the stabilization of proteins. *J. Phys. Chem. B* **120**, 4723–4731 (2016).
41. Robertson, A. D. & Murphy, K. P. Protein structure and the energetics of protein stability. *Chem. Rev.* **97**, 1251–1268 (1997).
42. Prabhu, N. V. & Sharp, K. A. Heat capacity in proteins. *Annu. Rev. Phys. Chem.* **56**, 521–548 (2005).
43. Hiraoka, S., Harano, K., Nakamura, T., Shiro, M. & Shionoya, M. Induced-fit formation of a tetrameric organic capsule consisting of hexagram-shaped amphiphile molecules. *Angew. Chem. Int. Ed.* **48**, 7006–7009 (2009).
44. Murphy, K. P. & Freire, E. Thermodynamics of structural stability and cooperative folding behavior in proteins. *Adv. Protein Chem.* **43**, 313–361 (1992).
45. Durchschlag, H. Determination of the partial specific volume of conjugated proteins. *Colloid Polym. Sci.* **267**, 1139–1150 (1989).
46. Ratnaparkhi, G. S. & Varadarajan, R. Thermodynamic and structural studies of cavity formation in proteins suggest that loss of packing interactions rather than the hydrophobic effect dominates the observed energetics. *Biochemistry* **39**, 12365–12374 (2000).
47. Matsuura, Y. et al. Role of charged residues in stabilization of *Pyrococcus horikoshii* CutA1, which has a denaturation temperature of nearly 150 °C. *FEBS J.* **279**, 78–90 (2012).
48. Matsuura, Y. et al. Thermodynamics of protein denaturation at temperatures over 100 °C: CutA1 mutant proteins substituted with hydrophobic and charged residues. *Sci. Rep.* **5**, 15545 (2015).

Acknowledgements

We thank Prof. H. Kawai (Tokyo University of Science) for a part of the ITC measurements. We thank Dr. H. Hamada (Malvern Instruments) for the DSC measurements. This research was supported by JSPS Grants-in-Aid for Scientific Research on Innovative Areas "Dynamical Ordering of Biomolecular Systems for Creation of Integrated Functions" (25102001, 25102005, 16H00770, and 16H00780) and the Joint Studies Program in the Okazaki BIONEXT project of National Institutes of Natural Sciences.

Author contributions

Y.-Y.Z., T.Koj., and S.H. conceived the project. S.H. prepared the manuscript and all the authors discussed the results and commented on the manuscript. Y.-Y.Z. synthesized all the GSAs and carried out all the NMR, ITC, and PSV measurements and a part of the molecular mechanics calculations. K.O. synthesized **BM** GSA and investigated its self-assembly in D_2O. T.Koi., T.M., and M.T. carried out part of the molecular mechanics calculations. K.I. and S.U. carried out mass measurements.

Additional information

Supplementary information accompanies this paper at https://doi.org/10.1038/s42004-018-0014-2.

Competing interests: The authors declare no competing interests.